ANL/MSD/CP-102632

RECEIVED
SEP 12 2000
OSTI

Increased Medium-Range Order in Amorphous Silicon with Increased Substrate Temperature

P. M. Voyles (Dept. of Physics, Univ. of Ill. and NEC Res. Institute),
J. E. Gerbi (Dept of Mat. Sci. & Eng. and Coordinated Sci. Lab. U. of I.),
M. M. J. Treacy (NEC Res. Institute),
J. M. Gibson (Argonne National Laboratory), and
J. R. Abelson (Dept of Mat. Sci. & Eng. and Coordinated Sci. Lab. U. of I.),

The submitted manuscript has been created by the University of Chicago as Operator of Argonne National Laboratory ("Argonne") under Contract No. W-31-109-ENG-38 with the U.S. Department of Energy. The U.S. Government retains for itself, and others acting on its behalf, a paid-up, nonexclusive, irrevocable worldwide license in said article to reproduce, prepare derivative works, distribute copies to the public, and perform publicly and display publicly, by or on behalf of the Government.

Distribution:
PRS (3)
J. M. Gibson (5)
L. E. Rehn
J. Coble
File

For submission to a special issue of J. Non-Crystalline Solids,
A. C. Wright and G. N. Greaves, Eds.
8th International Conference on the Structure of Non-Crystalline Materials, University of Wales, Aberystwyth, August 6-11, 2000

Work supported by the U.S. Department of Energy, Office of Science under contract No. W-31-109-Eng-38.

DISCLAIMER

This report was prepared as an account of work sponsored by an agency of the United States Government. Neither the United States Government nor any agency thereof, nor any of their employees, make any warranty, express or implied, or assumes any legal liability or responsibility for the accuracy, completeness, or usefulness of any information, apparatus, product, or process disclosed, or represents that its use would not infringe privately owned rights. Reference herein to any specific commercial product, process, or service by trade name, trademark, manufacturer, or otherwise does not necessarily constitute or imply its endorsement, recommendation, or favoring by the United States Government or any agency thereof. The views and opinions of authors expressed herein do not necessarily state or reflect those of the United States Government or any agency thereof.

DISCLAIMER

Portions of this document may be illegible in electronic image products. Images are produced from the best available original document.

Increased Medium-Range Order in Amorphous Silicon with Increased Substrate Temperature

P. M. Voyles,[1,2] J. E. Gerbi,[3] M. M. J. Treacy,[2] J. M. Gibson,[4] and J. R. Abelson[3]

[1]Dept. of Physics, University of Illinois, 1110 W. Green St., Urbana, IL 61801
[2]NEC Research Institute, 4 Independence Way, Princeton, NJ 08540
[3]Dept. of Materials Science and Engineering and Coordinated Science Laboratory, University of Illinois, 1110 W. Springfield Ave., Urbana, IL 61801
[4]Materials Science Division, Argonne National Laboratory, 9700 Cass Ave., Argonne, IL 60439

Using fluctuation electron microscopy, we have measured the medium-range order of magnetron sputtered silicon thin films as a function of substrate temperature from the amorphous to polycrystalline regimes. We find a smooth increase in the medium-range order of the samples, which we interpret in the context of the paracrystalline structural model as an increase in the size of and/or volume fraction occupied by the paracrystalline grains. These data are counter to the long-standing belief that there is a sharp transition between amorphous and polycrystalline structures as a function of substrate temperature.
PACS numbers: 61.43.Dq, 68.55.Jk, 64.70.Kb

I. INTRODUCTION

Medium-range order (MRO) in amorphous silicon (a-Si) is any structure that lies between the short-range (2–5 Å) order and long-range (> 300 Å) disorder a-Si is known to have from x-ray diffraction experiments [1]. There are important physical properties that involve structure at medium-range (~10 Å) length scales, such as the vibrational structure of a-Si [2,3]. In this paper we deal with the process of crystallization during thin film growth. Since the observations of Vepřek *et. al.* [4,5], it has been believed that there is an abrupt structural transition between the amorphous and polycrystalline phases of silicon in thin films deposited at increasing substrate temperature. Vepřek explained this transition in terms of an observed lattice dilation in the polycrystalline phase, which, when it becomes large enough, makes that phase energetically unstable.

Vepřek's measurements were made by x-ray diffraction. It is known, however, that there are many qualitatively different structures that have the same structure factor [6,7] and are thus indistinguishable by x-ray diffraction. Crystallization, which involves the collective action of thousands or millions of atoms, is essentially a question of MRO. Because of the isotropic nature of a-Si and the large-scale averaging involved, diffraction experiments contain little information about the structure of a-Si at length scales longer than ~8 Å.

We have developed fluctuation microscopy to address just this sort of question. Fluctuation microscopy is a quantitative transmission electron microscopy (TEM) technique that is sensitive to MRO in disordered materials. In fluctuation microscopy, we measure the normalized variance of low-resolution, hollow-cone dark field electron micrographs, defined as

$$V(k,Q) = \frac{\langle I^2(k,Q)\rangle}{\langle I(k,Q)\rangle^2} - 1, \qquad (1)$$

where $I(k,Q)$ is the image intensity, and $\langle\ \ \rangle$ indicates averaging over the image.

A dark-field micrograph is formed only with diffracted radiation. We can qualitatively understand a low-resolution dark-field micrograph as a position-resolved map of the diffracted intensity from mesoscopic volumes in the sample [8]. k and Q are the parameters that describe the imaging conditions. k is the dark-field scattering vector magnitude, which selects the diffracting condition for the radiation that is allowed into the image. Q is the microscope resolution, which controls the lateral extent of the mesoscopic volumes which extend through the thickness of the sample.

To see why $V(k,Q)$ is sensitive to MRO, consider the diffraction map image of two prototypical samples [8]. The first sample is a collection of atoms at random positions. All mesoscopic volumes of this sample will have statistically similar structures, so their corresponding diffracted intensities will be similar. That describes a diffraction map with only small deviations from the mean and a low variance. In addition, if we change the diffracting condition k or the resolution Q, the variance will not change significantly, since there are no dominant pair spacings or length scales in the sample to change the diffraction. The second sample is a compact of ordered clusters which are randomly oriented with respect to the electron beam. Some mesoscopic volumes in this sample will diffract strongly if they contain a cluster oriented at a Bragg condition, while others will diffract weekly if they do not. That describes a diffraction map with a high variance. In this case, if we vary the diffraction condition k, the variance will change as we pass through maxima and minima in the structure factor of the clusters. If we vary Q, the variance will also change as we include more

and more of each cluster and eventually more than one cluster in each sampling volume.

This example shows that, qualitatively, a low variance with little structure in k and Q is the signature of little or no MRO, and a high variance with significant structure in k and Q is the signature of significant MRO. Quantitatively, the imaging is a set of convolutions and the sensitivity to MRO derives from the three- and four-body atom distribution functions [9]. So far we only have the experimental capability to vary k at fixed Q, so all our results are plotted as $V(k)$. $V(k)$ gives information about the degree of MRO from the height of its peaks and the internal structure of any ordered regions from the peak positions.

Our previous fluctuation microscopy experiments have led us to the conclusion that vacuum deposited amorphous silicon and germanium thin films are paracrystalline [10,11]. A paracrystalline structure consists of small (< 30 Å diameter), highly strained, topologically crystalline grains [12] which may sit in a more disordered matrix. Because the grains are strained, few of the atoms sit on the their crystalline lattice positions, and the material appears amorphous to diffraction. However, the grains have subtle internal ordering which contributes MRO to the structure. Continuous random network models do not have enough MRO to be consistent with our fluctuation microscopy results [10].

The paracrystalline model suggests a reinterpretation of the x-ray data. Instead of an abrupt change in the structure of the films, Vepřek *et. al.* observed an abrupt change in the sensitivity of x-ray diffraction to that structure. Roughly speaking, once the strain field from the grain boundaries extends all the way across each grain, the grains disappear from diffraction measurements. There ought to be, however, a continuous evolution in the MRO of the samples. We have observed just such a continuous evolution by fluctuation microscopy.

II. EXPERIMENT

We have examined five Si thin films deposited by dc magnetron sputtering onto single-crystal NaCl substrates held at various temperatures. Samples were sputtered in a 1.8 mTorr argon atmosphere at a sputtering current of 0.3 A and a substrate floating voltage of 18 eV. The growth chamber has a base pressure of 10^{-7} Torr. Deposition conditions for each sample are given in Table I.

The NaCl substrate was chosen to aid in TEM sample preparation for fluctuation microscopy. Due to its quantitative nature, fluctuation microscopy cannot tolerate additional scattering due to glue and or residual substrate, and requires a large, thin (< 300 Å), uniform-thickness, free-standing sample. In addition, we wish to use only chemical thinning during the sample preparation, as dimpling or ion milling may introduce uncontrolled and poorly-understood artifacts into the sample. Sample preparation from a film on NaCl fulfills these requirements. We simply immerse the sample in deionized water, and the film floats off on the surface and is caught on a 1000 mesh Cu electron microscopy grid.

TABLE I. Deposition parameters of the samples. T_s is the substrate temperature, r_d is the deposition rate, and t is the thickness.

T_s (°C)	r_d (Å/s)	t (Å)
200	1.2	230
250	1.1	250
300	1.0	200
350	0.9	270
440	1.3	240

Fluctuation microscopy experiments were performed in a Hitachi H9000NAR TEM equipped with a Gatan CCD camera and a custom hollow-cone illumination unit and acquisition automation system. The microscope was operated at 200 kV accelerating voltage and a resolution of $0.61/Q = 15$ Å. Each $V(k)$ trace is the average of at least ten different sets of measurements, quoted with one standard deviation of the mean error bars. The images have been Fourier filtered and corrected for the camera modulation transfer function, sample thickness variations, and incoherent variance, as previously described [13].

Plane wave selected area electron diffraction measurements were also made in the H9000. Each trace is the cylindrical average of the acquired diffraction pattern image, further averaged over at least two different areas of the sample.

The morphology of the samples as observed by standard TEM was nonuniform, showing a degree of agglomeration into Si "beads" that increased with increasing substrate temperature. The characteristic size of the beads was ~350 Å, considerably larger than the 15 Å characteristic sampling volume used in the fluctuation microscopy measurements. The primary effect of the film morphology is to contribute a k-independent offset to the $V(k)$ data, which we subtract off [13]. For some of the samples, the incoherent variance subtraction procedure overcompensated, leading to a fictitious negative variance. All the $V(k)$ curves have therefore been vertically offset by 0.06 so that the minimum quoted variance is zero: this does not affect our conclusions, which are based on the relative magnitude of the peaks in $V(k)$.

III. RESULTS

Figure 1 shows the transmission electron diffraction intensity from the samples. This is the electron equiva-

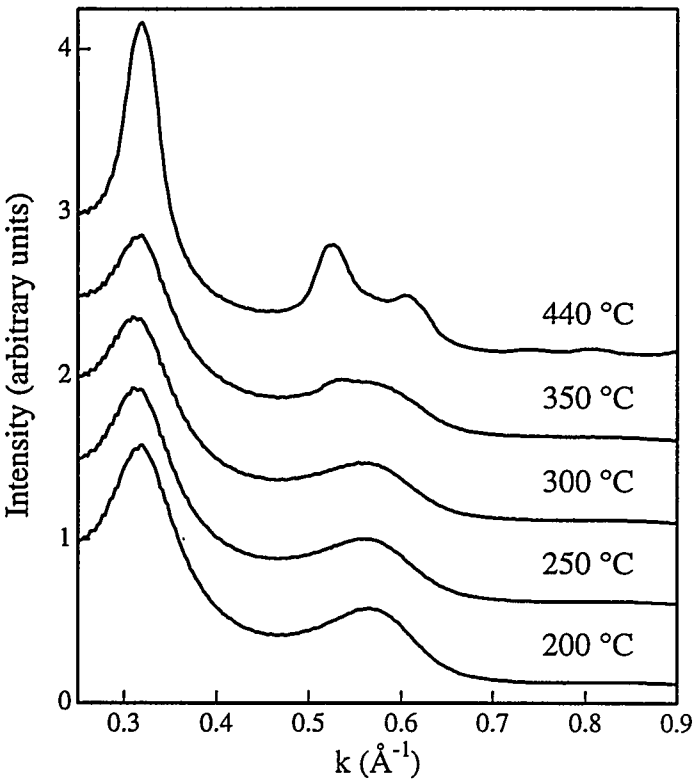

FIG. 1. Transmission electron diffraction data for the samples. Each trace if offset by 0.5 from the trace below.

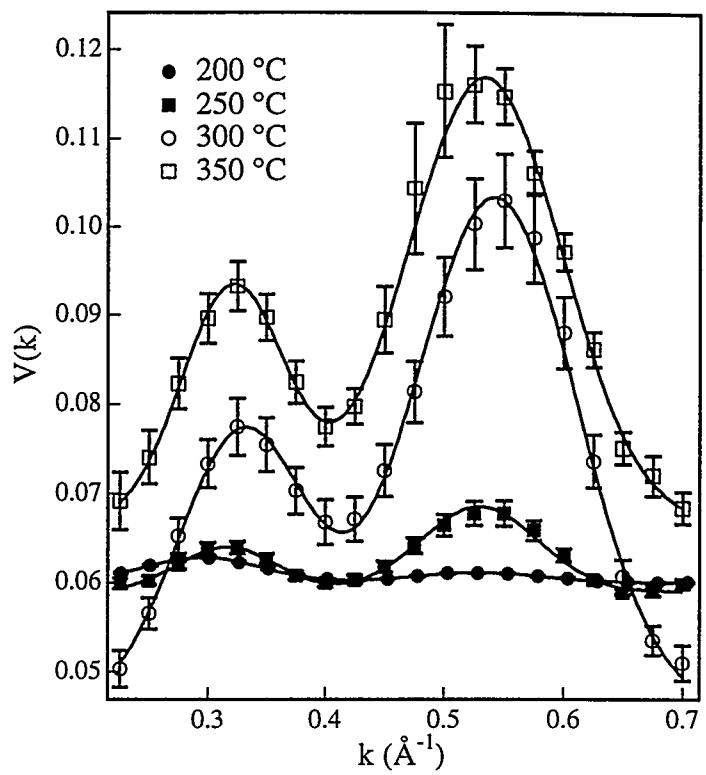

FIG. 2. Fluctuation microscopy $V(k)$ data for the amorphous phase (T_s = 200–350 °C) samples.

lent of standard x-ray diffraction,* and gives information about the phase of the sample. The T_s = 200–300 °C samples all show the characteristic pattern of a-Si, with peaks at $k = 0.31$ Å^{-1} and $k = 0.57$ Å^{-1} [1]. The third peak is too small to be detected simultaneously with the first peak within the dynamic range of the CCD camera. The 440 °C sample shows peaks at $k = 0.31$ Å^{-1}, 0.53 Å^{-1}, and 0.61 Å^{-1}. The last two peaks correspond to the crystalline Si ⟨220⟩ and ⟨311⟩ reflections, indicating that the 440 °C sample is polycrystalline. The 350 °C sample has a small crystalline volume fraction, on the order of 0.1 %, as indicated by the shoulder on the low-k side of the $k = 0.57$ Å^{-1} peak, which is associated with a weak ⟨220⟩ reflection.

Figure 2 shows fluctuation microscopy data for the amorphous phase samples, T_s = 200–350 °C. We observe a monotonic increase in the height of both of the peaks with increasing substrate temperature from T_s = 200–300 °C. There is a reversal in the relative heights of the two peaks, with the first peak higher than the second in the 200 °C sample, and the second higher than the first is all the higher T_s samples. The 200 °C sample also shows a small shift in the positions of the first peak towards lower k.

The 350 °C sample has the same peak-to-dip $V(k)$ magnitude as the 300 °C sample. The k-independent offset of this trace is due to a lack of accuracy in our incoherent variance correction scheme as applied to this data set. The second peak in $V(k)$ is shifted slightly towards lower k in this data compared to the lower temperature data.

All of the low-T_s data are well-fit by a sum of two Gaussians, one for each peak, and an additional k-independent offset parameter, giving

$$V(k) = h_1 \exp\left[\frac{(k-k_1)^2}{\Delta k_1^2}\right] + h_2 \exp\left[\frac{(k-k_2)^2}{\Delta k_2^2}\right] + v_0. \tag{2}$$

The solid lines in Figure 2 are fits to this form. The fit parameters are given in Table II. There is no physical reason for the Gaussian form; instead we believe that there are many contributions to the experimental peak shape which taken together give a Gaussian shape by the central limit theorem. The peak height parameters h_1 and h_2 bear out the observations already made. The shift of the first peak in the 200 °C sample is reflected in its k_1, but the shift of the second peak in the 350 °C sample is not reflected in its k_2. Note, however, that the

*For historical reasons, electron microscopists define $k = 1/\lambda$ instead of $k = 2\pi/\lambda$, so the k units throughout are 2π smaller than the x-ray units.

TABLE II. Parameters extracted from fitting $V(k)$ to Equation 2. h_1, h_2, and v_0 are, like $V(k)$, unitless.

T_s (°C)	$h_1 \times 10^3$	k_1 (Å^{-1})	Δk_1 (Å^{-1})	$h_2 \times 10^3$	k_2 (Å^{-1})	Δk_2 (Å^{-1})	$v_0 \times 10^3$
200	2.88 ± 0.07	0.295 ± 0.001	0.072 ± 0.002	1.12 ± 0.05	0.528 ± 0.002	0.079 ± 0.004	-0.03 ± 0.04
250	5.0 ± 0.5	0.316 ± 0.003	0.059 ± 0.006	9.5 ± 0.8	0.530 ± 0.003	0.069 ± 0.005	-0.9 ± 0.3
300	31 ± 3	0.330 ± 0.005	0.079 ± 0.007	58 ± 3	0.542 ± 0.004	0.096 ± 0.006	-14 ± 3
350	27 ± 3	0.322 ± 0.004	0.063 ± 0.007	50 ± 2	0.534 ± 0.003	0.091 ± 0.005	7.0 ± 2.0
440[a]	310 ± 50	0.305 ± 0.004	0.041 ± 0.005	300 ± 50	0.502 ± 0.004	0.056 ± 0.006	-38.0 ± 7.0
440[b]	310 ± 40	0.304 ± 0.004	0.046 ± 0.006	400 ± 100	0.485 ± 0.006	0.041 ± 0.009	60 ± 10

[a]Fit to two Gaussian peaks.
[b]Fit to three Gaussian peaks. Fit parameters for the third peak are given in the text.

fit curve passes below all of the data points on the low-k side of the 350 °C second peak. There may also be some sensitivity to the initial fit parameters used to start the iterative non-linear fitting procedure.

Figure 3 shows $V(k)$ for the polycrystalline 440 °C sample. The overall magnitude of $V(k)$ is ~4 times larger than that of the 350 °C sample. The second peak has shifted to lower k, and we believe there is a third peak developing at higher k. The dashed line in Figure 3 is a fit to the double-peak form of Equation 2, which is unsatisfactory. The solid line is a fit to a triple-peak form, which is much better. Table II gives the fit parameters for the double-peak form and the first two peaks of the triple-peak form. The fit parameters for the third peak are $h_3 = 0.1 \pm 0.05$, $k_3 = 0.56 \pm 0.06$ and $\Delta k_3 = 0.08 \pm 0.06$. The appearance of the third peak is associated with a splitting of the second peak into contributions from crystalline ⟨220⟩ and ⟨311⟩ reflections. The error bars are larger in this data than that in Figure 2 because the polycrystalline grain size is 100-200 Å, so there are far fewer structural units in each 0.025 μm^2 image than in the amorphous sample images and the statistical sampling is poorer.

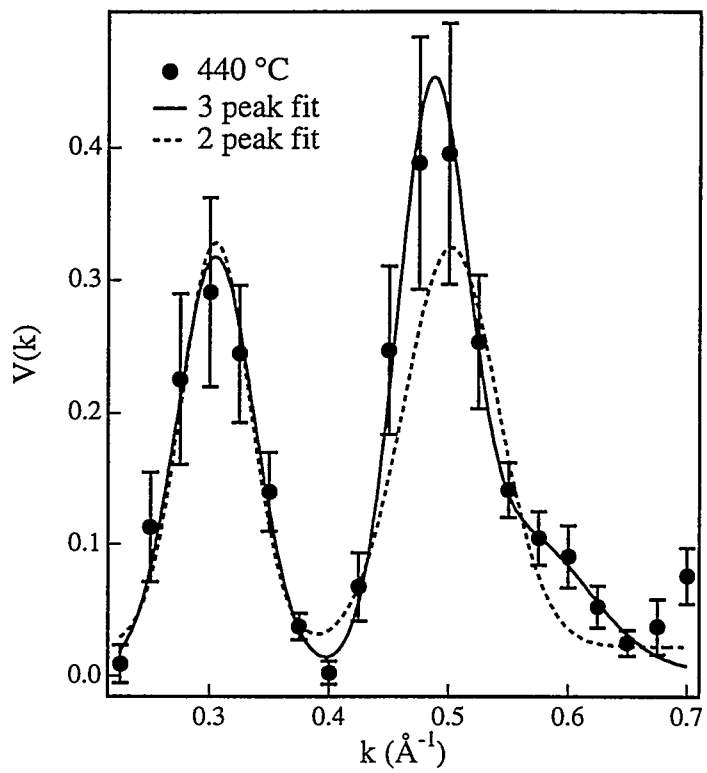

FIG. 3. Fluctuation microscopy $V(k)$ data for the polycrystalline sample. Note the increase in vertical scale with respect to Figure 2.

IV. DISCUSSION

The data presented in Section III have shed new light on the general interpretation of $V(k)$ data. $V(k)$ is sensitive to fluctuations in the diffraction intensity, rather than the magnitude of the intensity itself, so $V(k)$ for the polycrystalline sample is large because the crystalline grains are localized, high-intensity scatterers. When we find a k that corresponds to the diffracting condition for a grain, it diffracts strongly, while everything around it does not. The same thing happens in the amorphous samples, but at a smaller length scale and lower magnitude.

For all but the T_s = 200 °C sample, the peak at the ⟨220⟩ position is higher in $V(k)$ than the peak at the ⟨111⟩ position, indicating that the fluctuations in the ⟨220⟩ diffraction are larger. Figure 4 provides an explanation of this phenomena. It shows the diffracted intensity into the indicated ⟨111⟩ and ⟨202⟩ reflections from an eight atom cluster as a function of the cluster's dihedral angle. The connecting bond ⟨111⟩ vector is not changed by the dihedral angle rotation, so its diffracted intensity is constant. The ⟨202⟩ intensity changes with the dihedral angle, having a maximum at 60°, which is the dihedral angle typical of crystalline Si. There are three other ⟨111⟩ family vectors, such as $\langle 11\bar{1} \rangle$, in this cluster which will vary with the dihedral angle, and there are seven more ⟨220⟩ family vectors, such as $\langle 20\bar{2} \rangle$, but overall, the ⟨220⟩ reflections shows more variation in intensity with the dihedral angle than the ⟨111⟩ reflections.

Consider a structure with a spatially uniform random distribution of dihedral angles. The diffracted intensity from the mesoscopic volumes of such a structure will remain close to the average values of the two curves in

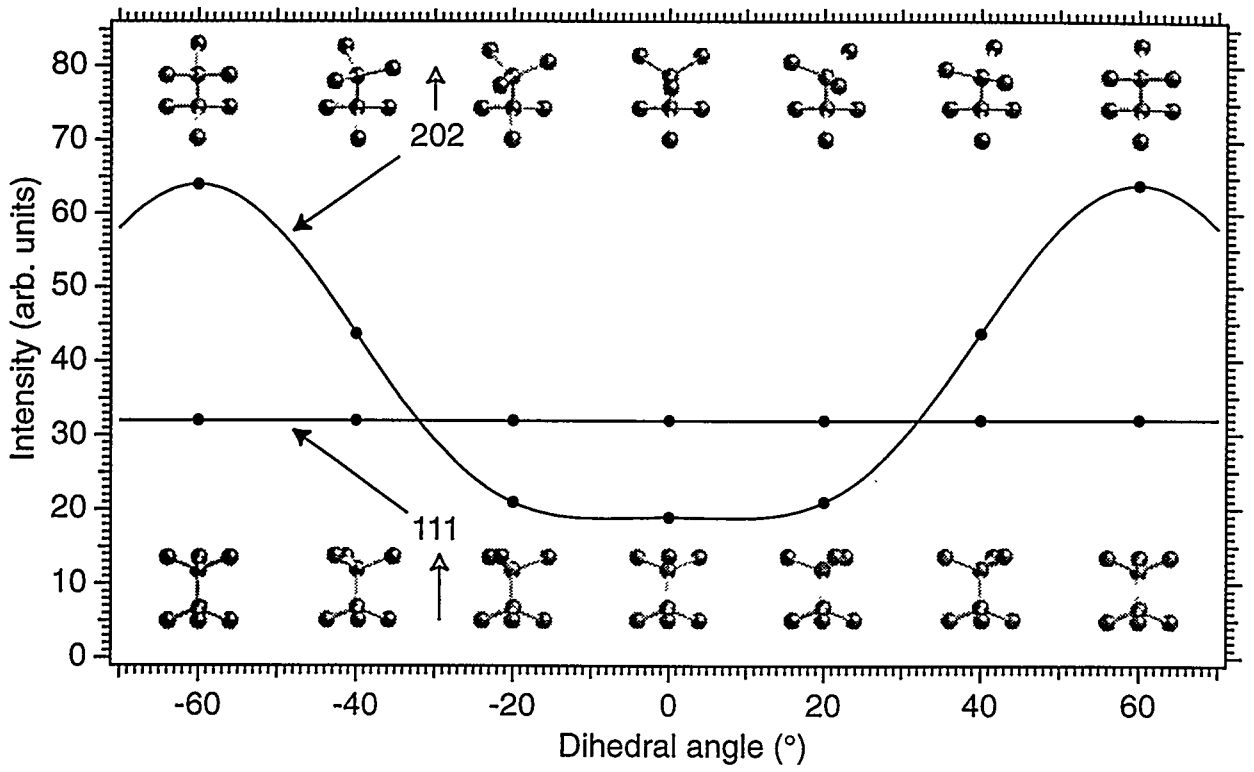

FIG. 4. The variation in diffracted intensity from a ⟨111⟩ and a ⟨220⟩ reflection of an eight atom cluster with the cluster's central dihedral angle. Pictures of the cluster at different dihedral angles are shown across the top and bottom. The open arrow lines indicate the direction of the diffraction vector in the pictures. The solid arrow lines connect the pictures and the graph traces.

Figure 4. Now consider a structure with some regions in which the dihedral angles show a greater tendency towards the crystalline value of 60°. The ⟨111⟩ reflection intensity is not much different inside or outside these regions, since it is relatively insensitive to dihedral angle ordering. The ⟨220⟩ intensity, however, becomes significantly larger in the ordered regions and remains lower outside them. Thus the fluctuations in the diffracted intensity are larger in the ⟨220⟩ reflection, and the second peak in $V(k)$ is greater in magnitude than the first peak.

This is what we believe is occurring in the samples we have examined as a function of T_s. The monotonic increase in both of the peak heights with T_s from T_s = 200–300 °C is an indicator of increasing MRO, as is the reversal of the relative heights. We believe the MRO takes the form of paracrystalline grains which are topologically crystalline [12], although distorted by strain. Those regions grow larger and/or occupy a greater volume fraction with increasing T_s. One expression of the increased MRO of the grains is a preference for crystalline Si dihedral angles, which leads to the observed reversal in the peak heights with increasing order. The further ordering of the 350 °C sample with the introduction of a small crystalline volume fraction is indicated by the shift in the second peak from the amorphous towards the crystalline diffracting condition. As shown in Figure 1, these changes in MRO are not detected by diffraction.

These data are evidence that there is a smooth structural transition between amorphous and polycrystalline structures in Si as a function of T_s. This occurs naturally within the paracrystalline model: the grains simply grow larger and larger with increasing T_s until they become visible to diffraction and we consider the sample to be polycrystalline. It is important to note that a paracrystal a metastable, not equilibrium, state. Theoretically, there may be a phase transition between the polycrystalline state and some disordered state, meaning that the equilibrium energy of the disordered state could be lower than the polycrystalline state under the right conditions. We believe, however, that a real film deposited under highly non-equilibrium conditions of high deposition rate and low substrate temperature will never reach that equilibrium disordered state. Instead, it becomes trapped in a metastable state that is locally crystalline, but globally disordered and best characterized as paracrystalline.

Finally, these data shed some light on some of our previous observations. First, the lowest temperature T_s = 200 °C data are consistent with our previous measurements on a-Si and hydrogenated a-Si (a-Si:H) [11,14], indicating that those results were not an artifact of the aluminum foil substrate on which the films were grown. Second, we have reported a difference in MRO between a-

Ge and a-Si thin films [10]. The a-Ge films look more like the higher-T_s a-Si films we have examined here, in that the second peak in $V(k)$ is higher than the first, so those results may be due to differences in the homologous substrate temperature, rather than some fundamental property of the elements. Finally, we have reported that hot-wire CVD (HWCVD) a-Si:H has similar MRO to other forms of a-Si:H [11]. However, the HWCVD sample we examined was deposited at 380 °C, which, compared to the 350 °C sample here, makes it remarkable for having so little MRO, rather than having more MRO than other forms of a-Si:H as has been suggested based on x-ray data [15]. Further experiments are needed to completely understand these observations.

V. CONCLUSIONS

We have examined with fluctuation microscopy the medium-range order (MRO) of magnetron sputtered amorphous silicon (a-Si) as a function of substrate temperature T_s over a range of temperatures that produce amorphous and polycrystalline structures. We observe a smooth increase in MRO with increasing T_s. The MRO increases even in the lowest temperature samples with $T_s = 200$, 250, and 300 °C which have indistinguishable transmission electron diffraction spectra.

We explain these results in terms of the paracrystalline model which consists of small, topologically crystalline grains which may be in a disordered matrix. The increasing MRO of the samples is due to the increasing size of and/or volume fraction occupied by the paracrystalline grains. Because the grains are strained, few of the atoms sit on their crystalline lattice positions, and the structure remains amorphous to diffraction experiments until the grains exceed some critical size. In this model, the earlier reports of a sharp transition between polycrystalline and amorphous Si as a function of T_s using x-ray diffraction [4,5] are a result of a sharp transition in the sensitivity of x-ray diffraction to the relevant structure, rather than a sharp transition in the structure itself.

VI. ACKNOWLEDGEMENTS

We thank Peggy Bisher for technical assistance. P. M. V. acknowledges the support of the National Science Foundation under grant DMR 97-03906. J. E. G. and J. R. A. acknowledge the support of the National Renewable Energy Laboratory under subcontract ADD-9-18668.

[1] K. Laaziri, S Kycia, S. Roorda, M. Chicoine, J. L. Robertson, J. Wang, and S. C. Moss, Phys. Rev. Lett. **82**, 3460 (1999); Phys. Rev. B **60**, 13520 (1999).

[2] A. P. Sokolov and A. P. Shebanin, Sov. Phys. Semicond. **24**, 720 (1990).

[3] G. Morell, R. S. Katiyar, S. Z. Weisz, J. Jia, J. Shinar, and I. Balberg, J. Appl. Phys. **78**, 5120 (1995).

[4] S. Vepřek, Z. Iqbal, H. R. Oswald, F.-A. Sarott, J. J. Wagner, and A. P. Webb, Sol. State Comm. **39**, 509 (1981).

[5] S. Vepřek, Z. Iqbal, and F.-A. Sarott, Phil. Mag. B **45**, 137 (1982).

[6] J. M. Gibson and M. M. J. Treacy, Phys. Rev. Lett. **78**, 1074 (1997).

[7] N. Mousseau and L. J. Lewis, Phys. Rev. Lett. **78**, 1484 (1997).

[8] P. M. Voyles, J. M. Gibson, and M. M. J. Treacy, J. Electron Microscopy **49**, 259 (2000).

[9] J. M. Gibson, M. M. J. Treacy, and P. M. Voyles, Ultramicroscopy **83**, 169 (2000).

[10] J. M. Gibson, M. M. J. Treacy and P. J. Keblinski, J. Non-Cryst. Solids **231**, 99 (1998).

[11] P. M. Voyles, M. M. J. Treacy, H-C. Jin, J. R. Abelson, J. M. Gibson, J. Yang, S. Guha, and R. S. Crandall, Mat. Res. Soc. Symp. Proc. **609**, to be published.

[12] M. M. J. Treacy, P. M. Voyles, and J. M. Gibson, J. Non-Cryst. Sol. **266–269**, 150 (2000).

[13] P. M. Voyles, M. M. J. Treacy, J. M. Gibson, H-C. Jin, and J. R. Abelson, Mat. Res. Soc. Symp. Proc. **589**, to be published..

[14] J. M. Gibson, M. M. J. Treacy, P. M. Voyles, H-C. Jin, and J. R. Abelson, Appl. Phys. Lett. **73**, 3093 (1998).

[15] A. H. Mahan, D. L. Williamson, and T. E. Furtak, Mat. Res. Soc. Symp. Proc. **467**, 657 (1997).